*SQU Journal for Science*, 2018, 23(1), 56-67 DOI: http://dx.doi.org/10.24200/squjs.vol23iss1pp56-67
Sultan Qaboos University

# Heat Transfer in $Fe_3O_4$-$H_2O$ Nanofluid Contained in a Triangular Cavity Under a Sloping Magnetic Field

**Mohammad M. Rahman**

*Department of Mathematics and Statistics, College of Science, Sultan Qaboos University, Box 36, Al-Khod 123, Sultanate of Oman. Email:mansur@squ.edu.om*

**ABSTRACT:** Numerical simulation is performed to explore the convective heat transfer characteristics of $Fe_3O_4$-$H_2O$ nanofluid contained in a right-angle triangular cavity considering three types of thermal boundary conditions at the bottom wall. No heat is allowed to escape through the insulated vertical wall, whereas the inclined wall is kept colder than the bottom one. A sloping magnetic field whose strength is unvarying acts upon the cavity. The physical model is converted to the mathematical form through coupled highly nonlinear partial differential equations. These equations are then transformed into the non-dimensional form with the help of a group of transformations of variables. A very robust pde solver COMSOL Multiphysics that uses the finite element method (FEM) of Galerkin type is applied to carry out the numerical calculation. Heat transfer escalation through middling Nusselt number at the lowermost cavity wall is explored for diverse model parameters and thermal circumstances. The outcomes lead us to conclude that a higher degree of heat transfer is accomplished by reducing the dimension of nanoparticles and aggregating the buoyancy force through the Rayleigh number. It is highest when there is a magnetic field leaning angle of $90^0$ and the lowermost wall is heated homogenously.

**Keywords:** Nanofluid, Free convection, Triangular cavity, Sloping magnetic field, FEM

## انتقال الحرارة في حاوية مثلثة تحوي المائع النانوي لأكسيد الحديد- ماء تحت تأثير مجال مغناطيسي منزلق

**محمد منصور رحمان**

**الملخص:** تم تنفيذ محاكاة عددية لتوضيح خصائص انتقال الحرارة الحملي للمائع النانوي لأكسيد الحديد – ماء داخل حاوية على شكل مثلث قائم الزاوية تتضمن ثلاثة أنواع من خصائص الحدود الحرارية للضلع الأسفل. ونفترض أن تهريب الحرارة عبر الضلع الرأسي غير مسموح به بحيث يبقى الضلع المائل أبرد من الضلع السفلي. ووجود مجال مغناطيسي منزلق ثابت الشدة يؤثر على الحاوية. وتم تحويل النموذج الفيزيائي إلى شكل رياضي بمعادلات تفاضلية جزئية وغيرخطية. وحولت تلك المعادلات الى شكل بدون وحدات ومساعدة مجموعة من المتغيرات التحويلية. لإجراء الحسابات العددية تم استخدام برنامج الحاسوب كومسول ملتيفيزكس (COMSOL Multiphysics) لحل المعادلات التفاضلية الجزئية، حيث أن البرنامج يعمل بطريقة العناصر المحدودة (FEM) من نوع جالاركن. ويكون تصعيد انتقال الحرارة عبر اعتدال رقم نسلت (Nusselt number) من خلال جدار الحاوية الأدنى الذي تم اكشافه لنموذج مختلف من المعاملات و الظروف الحرارية. كشفت النتائج أن انتقال الحرارة بدرجة عالية يصحبه انخفاض في حجم الذرات النانوية وتجمع قوة الطفو عبر رقم ريليه (Rayleigh number) . وتكون الدرجة العليا عندما يميل المجال المغناطيسي بزاوية 90 درجة وتسخين متجانس للجدار السفلي.

**الكلمات المفتاحية:** مائع نانوي، حمل حراري، حاوية مثلثة، حقل مغناطيسي منزلق، طريقة العناصر المحدودة.

## Nomenclature

| | | | |
|---|---|---|---|
| $a$ | wave amplitude (m) | Ra | Rayleigh number |
| $A$ | dimensional wave amplitude | $T$ | temperature (K) |
| $AR$ | aspect ratio | $u, v$ | velocity components ($ms^{-1}$) |
| $\mathbf{B}$ | magnetic field vector | $U, V$ | nondimensional velocity components |
| $B_0$ | magnitude of the magnetic field ($NmA^{-1}$) | $x, y$ | coordinates (m) |
| $c_p$ | specific heat at constant pressure ($Jkg^{-1}K^{-1}$) | $X, Y$ | nondimensional coordinates |
| $C$ | nanoparticle volume fraction | | **Greek symbols** |
| $d$ | particle diameter (nm) | $\alpha$ | thermal diffusivity ($m^2s^{-1}$) |
| $D_B$ | coefficient of Brownian diffusion ($m^2s^{-1}$) | $\beta$ | coefficient of thermal expansion ($K^{-1}$) |
| $D_T$ | coefficient of thermophoretic diffusion ($m^2s^{-1}$) | $\gamma$ | magnetic field sloping angle ( $^0$ ) |
| $\mathbf{g}$ | gravity vector | $\delta$ | heat capacity ratio |
| $g$ | acceleration due to gravity ($ms^{-1}$) | $\theta$ | nondimensional temperature |
| $H$ | cavity height (m) | $\phi$ | normalized nanoparticle volume fraction |
| $Ha$ | Hartmann number | $\psi$ | stream function |
| $K$ | wave number | $\kappa$ | thermal conductivity ($Wm^{-1}K^{-1}$) |
| $L$ | cavity length (m) | $\rho$ | density ($kgm^{-3}$) |
| $Le$ | Lewis number | $\mu$ | dynamic viscosity ($kgm^{-1}s^{-1}$) |
| $Nb$ | Brownian diffusion parameter | $\upsilon$ | kinematic viscosity ($m^2s^{-1}$) |
| $Nr$ | buoyancy ratio parameter | $\rho c_p$ | heat capacity ($JK^{-1}m^{-3}$) |
| $Nt$ | thermophoresis parameter | | **Subscripts** |
| $Nu$ | Nusselt number | $av$ | average |
| $p$ | pressure (Pa) | $c$ | condition at cold wall |
| $P$ | nondimensional pressure | $f$ | base fluid |
| Pr | Prandtl number | $h$ | condition at heated wall |
| | | $p$ | solid nanoparticle |

## 1. Introduction

Natural convective heat transfer has extensive applications in numerous engineering areas such as air-cooling systems, chilling of electronic equipment, insulating buildings, harvesting solar thermal collectors, and the extraction of geothermal energy. Natural convective heat transfer may also transpire in buildings' roofs and attics. Many researchers [1–4] have investigated and tested findings both experimentally and numerically for heat transfer augmentation, considering natural convection within a square, rectangular, rhomboidal, annular and triangular cavity. Flack *et al*. [5-6] conducted experimental and numerical surveys to simulate convective heat transfer in a base fluid confined within a triangular enclosure. Later on many researchers were influenced by this ground breaking work and reported results on triangular cavities. The work of Akinsete and Coleman [7] on a pitched roof with a horizontally suspended ceiling inside the triangular enclosure showed that the heat transfer rate through the bottom wall escalates in the direction of the intersection of the hypotenuse and base. Keeping in mind the possible application of electronic components, Ridouane *et al*. [8] simulated natural convection heat transfer flow of air in a right-angled triangular container. They found that heat transfer reduction strongly depends on the decrease of the apex angle and the Rayleigh number. Varol et al. [9] conducted a numerical experiment to calculate natural convective heat transfer inside a triangular container having a non-isothermal bottom wall inserted in a permeable medium. They confirmed that heat transfer is enhanced when the upright and slanted walls are heated isothermally and the bottom wall is heated non-uniformly. The work of Basak *et al*. [10] within a triangular enclosure revealed that the heatlines are subjugated by conduction for a smaller Rayleigh number, whereas convection overrides conduction for a higher Rayleigh number. Yesiloz and Aydin [11] performed both an experimental and numerical study to scrutinize the heat relocation augmentation within a right-angled triangular enclosure which was heated from below and cooled from the side walls. They concluded that the rate of heat transfer intensifies when the Rayleigh number increases markedly.

A conducting fluid and an imposed magnetic field in the flow domain interact with each other and create a Lorentz force that in turn overwhelms the convection fluxes, and as a consequence fluid velocity diminishes. Exerting of such a magnetic field on the flow domain has extensive application in diverse circumstances. For example it could be used in metal casting, the extraction of geothermal energy, for controlling flow in fusion reactors, and growing crystals in liquids. In practical applications, the slopping of a magnetic field on the flow area is important for the proper functionality of the devices. The open literature reveals that a slopping magnetic field has a tendency to alter the fluid flow and subsequently the thermal enactment of a cavity (see Ozoe and Okada [12], Pirmohammadi and Ghassemi [13]). Sathiyammmoorthy and Chamkha [14] have investigated two-dimensional convective flow together with heat transfer inside a square cavity considering liquid gallium and an inclined magnetic field. They showed that heat transfer within the cavity is different for perpendicularly and flatly imposed magnetic fields. They further revealed that an applied magnetic field lowers heat transmission rates. Grosan *et al*. [15] conducted a numerical study on natural convective flow inside a rectangular cavity under the action of an inclined magnetic field. It was reported that the convective mode of heat transfer was prejudiced by the strength and alignment of the field. It was further shown that a horizontal magnetic field more effectively suppresses the flow, when compared to a field operating in an upright direction.

Studies of convective flow within cavities under the action of an imposed magnetic field usually considered fluids of low conductivity, which in turn limits the augmentation of heat transmission rates. However, in many practical applications, higher conductivity is required to transfer heat efficiently in sophisticated devices. A groundbreaking approach to enrich the conductivity is by mixing solid nanoparticles with the low-conductive fluid. This new type of engineered fluid is called a nanofluid (Choi [16]) and has substantially higher conductivity compared to the base fluid. Wide-ranging literature reviews, reporting the extensive applications of nanofluids are well documented by Wong and De Leon [17], Das *et al*. [18] and Mahian *et al*. [19], Kakac and Pramuanjaroenkij [20]. Uddin *et al*. [21] carried out an excellent review work on the ultimate features of nanofluids, along with their development and applications. They also established novel correlations for Brownian diffusion and thermophoresis in nanofluids. Plentiful results on nanofluids are available in different configurations of flow and thermal fields. Although there are lots of engineering and technological applications of the flow dynamics of nanofluids in triangular cavities, this has attracted far less attention from researchers. A mixed convective study on nanofluids inside a triangular cavity by Ghasemi and Aminossadati [22] showed that heat transference is enhanced by an increase of the nanoparticle loading. Billah *et al*. [23] investigated time-dependent buoyancy influenced by heat transfer augmentation of nanofluids inside a tilted right triangular cavity. They have shown that average Nusselt number as well as fluid temperature varies linearly with an increase of the nanoparticle volume fraction. Recently, Al Kalbani *et al*. [24] explored buoyancy-encouraged heat transmission inside a slanted square cavity occupied with nanofluids under the action of an inclined magnetic field. They have reported that Rayleigh number together with nanoparticle volume fraction intensifies heat transfer rate significantly. On the other hand, increased Hartmann number reduces the global heat transfer rate within the cavity. The critical geometry leaning angle to obtain the optimum heat transmission rate significantly hangs on the loading of the nanoparticles as well as on the magnetic field direction.

The above-stated models are well known one-component models, where the effects of thermophoresis and Brownian diffusion of nanoparticles have not been taken into consideration. Buongiorno [25] developed a two-component model considering these mechanisms of nanoparticles in connection with the relative velocity of the base-fluid. Sheremet and Pop [26] followed the model of Buongiorno, to study free convective heat transfer and fluid flow inside a triangular shaped cavity occupied with nanofluid implanted in a permeable medium. The outcomes of this study revealed that Rayleigh and Lewis numbers escalate the average Nusselt number, whereas it is diminished by the increase of buoyancy-ratio, thermophoresis, and Brownian diffusion parameters. Taking into consideration the slip mechanisms suggested by Buongiorno, Rahman *et al*. [27] investigated hydromagnetic flow characteristics of nanofluids inside an isosceles triangular shaped cavity, considering various thermal circumstances at the bottom wall. They reported that adaptable thermal circumstances substantially control the flow and updraft fields.

In keeping with the literature review, the author found that there remains a potential need to investigate the natural convective transport mechanism in $Fe_3O_4$-$H_2O$ nanofluid inside a right triangular cavity, considering different updraft boundary conditions and a sloping magnetic field. $Fe_3O_4$-water nanofluid has further high demand in technological applications such as in solar thermal collectors because of its upgraded thermophysical properties, convenience, and low production cost. In the present study, a finite element method of Galerkin type is used to carry out a numerical simulation. The simulated results such as streamlines, isotherms, and isoconcentrations are presented graphically, whereas the average Nusselt numbers are tabulated.

## 2. Physical and mathematical modeling

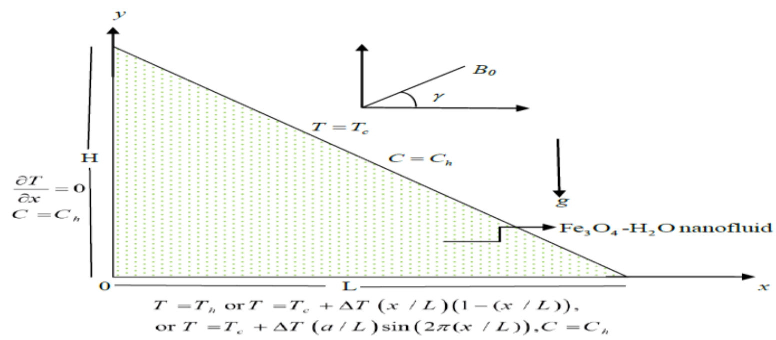


**Figure 1.** Diagram of the right triangular cavity with coordinate axes and boundary conditions.

We consider the two-dimensional time-independent viscous incompressible laminar flow of $Fe_3O_4$-$H_2O$ nanofluid confined in a right triangular cavity. The flow configuration and corresponding boundary conditions for flow and temperature are displayed in Fig. 1. The length of the bottom wall of the cavity is $L$ along the $x$-axis and its height is $H$ along the $y$-axis. The gravity $\mathbf{g}=[0,g]$ acts along the $y$-axis in the downward direction. We further consider that the temperature of the bottom wall varies uniformly $T=T_h$, parabolically $T=T_c+\Delta T\left(x/L\right)\left(1-\left(x/L\right)\right)$, and sinusoidally $T=T_c+\Delta T(a/L)\sin(Kx)$ where $\Delta T=T_h-T_c$, $a$ is the wave amplitude and $K=2\pi/L$ is the wave number. The inclined wall temperature we consider to be $T=T_c$ ($T_c<T_h$), keeping the vertical wall insulated. We assume that $Fe_3O_4$ nanoparticles distribute uniformly within the base fluid water and their concentration at all boundaries is constant such that $C=C_h$. So called "slip mechanisms", thermophoresis and Brownian diffusion are taken into consideration in the lack of chemical reaction to construct the mathematical model. Due to the tiny size of the nanoparticles, we may assume that $Fe_3O_4$ nanoparticles and water molecules are in local thermal equilibrium. A slopping magnetic field $\mathbf{B}=[B_0\cos\gamma, B_0\sin\gamma]$ is applied to the flow domain where $\gamma$ is the inclination angle with respect to the positive $x$-axis. The density variation of the nanofluid is tackled through incorporating the Boussinesq approximation in the momentum equation.

Following the above-noted suppositions, the governing equations of the model are ([27]-[28])

$$\frac{\partial u}{\partial x}+\frac{\partial v}{\partial y}=0 \tag{1}$$

$$\rho_f\left(u\frac{\partial u}{\partial x}+v\frac{\partial u}{\partial y}\right)=-\frac{\partial p}{\partial x}+\mu_f\left(\frac{\partial^2 u}{\partial x^2}+\frac{\partial^2 u}{\partial y^2}\right)+\sigma_f B_0^2\left(v\sin\gamma\cos\gamma-u\sin^2\gamma\right) \tag{2}$$

$$\begin{aligned}\rho_f\left(u\frac{\partial v}{\partial x}+v\frac{\partial v}{\partial y}\right)=-\frac{\partial p}{\partial y}+\mu_f\left(\frac{\partial^2 v}{\partial x^2}+\frac{\partial^2 v}{\partial y^2}\right)+\sigma_f B_0^2\left(u\sin\gamma\cos\gamma-v\cos^2\gamma\right)\\ +\left(1-C_c\right)\left(T-T_c\right)\rho_f\beta_f g-\left(C-C_c\right)\left(\rho_p-\rho_f\right)g\end{aligned} \tag{3}$$

$$u\frac{\partial T}{\partial x}+v\frac{\partial T}{\partial y}=\alpha_f\left(\frac{\partial^2 T}{\partial x^2}+\frac{\partial^2 T}{\partial y^2}\right)+\delta\left[D_B\left(\frac{\partial C}{\partial x}\frac{\partial T}{\partial x}+\frac{\partial C}{\partial y}\frac{\partial T}{\partial y}\right)+(D_T/T_c)\left(\left(\frac{\partial T}{\partial x}\right)^2+\left(\frac{\partial T}{\partial y}\right)^2\right)\right] \tag{4}$$

$$u\frac{\partial C}{\partial x}+v\frac{\partial C}{\partial y}=D_B\left(\frac{\partial^2 C}{\partial x^2}+\frac{\partial^2 C}{\partial y^2}\right)+(D_T/T_c)\left(\frac{\partial^2 T}{\partial x^2}+\frac{\partial^2 T}{\partial y^2}\right) \tag{5}$$

where $u$ and $v$ are velocity components along the $x$- and $y$- axes respectively, $p$ is the pressure and $\delta=\left(\rho c_p\right)_p/\left(\rho c_p\right)_f$ is the heat capacity ratio of nanoparticles and base fluid. For descriptions of other quantities, see the nomenclature.

Boundary conditions for flow, temperature and particle concentration are:

(i) At inclined wall ($x/L+y/H=1$):

$$u=v=0,\ T=T_c\ ,\ C=C_h. \tag{6}$$

(ii) At bottom wall ($y=0,\ 0\le x\le L$):

Type 1: $u=v=0,\ T=T_h,\ C=C_h.$ (7a)

Type 2: $u=v=0,\ T=T_c+\Delta T\left(x/L\right)\left(1-\left(x/L\right)\right),\ C=C_h.$ (7b)

Type 3: $u=v=0,\ T=T_c+\Delta T\left(\mathrm{a}/L\right)\sin\left(Kx\right),\ C=C_h.$ (7c)

(iii) At vertical wall ($x=0,\ 0\le y\le H$):

$$u=v=0,\ T_x=0,\ C=C_h. \tag{8}$$

To make equations (1)-(8) dimensionless, we use the following transformation of variables:

$$\left.\begin{aligned}&X=x/L, Y=y/L, U=uL/\alpha_f, V=vL/\alpha_f, P=pL^2/\rho_f\alpha_f^2,\\&\theta=(T-T_c)/(T_h-T_c), \phi=(C-C_c)/(C_h-C_c).\end{aligned}\right\} \tag{9}$$

Substituting (9) into (1)-(5), we obtain the following non-dimensional governing equations

$$\frac{\partial U}{\partial X}+\frac{\partial V}{\partial Y}=0 \tag{10}$$

$$U\frac{\partial U}{\partial X}+V\frac{\partial U}{\partial Y}=-\frac{\partial P}{\partial X}+\Pr\left(\frac{\partial^2 U}{\partial X^2}+\frac{\partial^2 U}{\partial Y^2}\right)+\Pr\mathrm{Ha}^2\left(V\sin\gamma\cos\gamma-U\sin^2\gamma\right) \tag{11}$$

$$U\frac{\partial V}{\partial X}+V\frac{\partial V}{\partial Y}=-\frac{\partial P}{\partial Y}+\Pr\left(\frac{\partial^2 V}{\partial X^2}+\frac{\partial^2 V}{\partial Y^2}\right)+Ra\Pr\left(\theta-Nr\phi\right)+\Pr\mathrm{Ha}^2\left(U\sin\gamma\cos\gamma-V\cos^2\gamma\right) \tag{12}$$

$$U\frac{\partial \theta}{\partial X}+V\frac{\partial \theta}{\partial Y}=\frac{\partial^2 \theta}{\partial X^2}+\frac{\partial^2 \theta}{\partial Y^2}+Nb\left(\frac{\partial \phi}{\partial X}\frac{\partial \theta}{\partial X}+\frac{\partial \phi}{\partial Y}\frac{\partial \theta}{\partial Y}\right)+Nt\left(\left(\frac{\partial \theta}{\partial X}\right)^2+\left(\frac{\partial \theta}{\partial Y}\right)^2\right) \tag{13}$$

$$U\frac{\partial \phi}{\partial X}+V\frac{\partial \phi}{\partial Y}=(1/Le)\left(\frac{\partial^2 \phi}{\partial X^2}+\frac{\partial^2 \phi}{\partial Y^2}\right)+(Nt/LeNb)\left(\frac{\partial^2 \theta}{\partial X^2}+\frac{\partial^2 \theta}{\partial Y^2}\right) \tag{14}$$

The boundary conditions (6)-(8) become

(i) At inclined wall $(X+Y/AR=1)$:

$$U=V=0,\ \theta=0,\ \phi=1. \tag{15}$$

(ii) At bottom wall ($Y=0,\ 0\le X\le 1$):

Type 1: $U=V=0,\theta=1,\ \phi=1.$ (16a)

Type 2: $U=V=0,\theta=X\left(1-X\right),\ \phi=1.$ (16b)

Type 3: $U=V=0,\theta=A\sin\left(2\pi X\right),\ \phi=1.$ (16c)

(iii) At vertical wall ( $X=0,\ 0\le Y\le AR$):

$$U=V=0,\frac{\partial \theta}{\partial X}=0,\ \phi=1. \tag{17}$$

The dimensionless parameters appearing in equations (11)-(14) are defined as:

Prandtl number $\Pr=\upsilon_f/\alpha_f$, Hartmann number $Ha=B_0L\sqrt{\sigma_f/\mu_f}$,

Rayleigh number $Ra=g\beta_f\left(1-C_c\right)\left(T_h-T_c\right)L^3/\alpha_f\upsilon_f$,

Buoyancy ratio parameter $Nr=\left(\rho_p-\rho_f\right)\left(C_h-C_c\right)/\rho_f\beta_f\left(T_h-T_c\right)\left(1-C_c\right)$,

Thermophoresis parameter $Nt=\delta D_T\left(T_h-T_c\right)/T_c\alpha_f$,

Brownian motion parameter $Nb=\delta D_B\left(C_h-C_c\right)/\alpha_f$,

Lewis number $Le=\alpha_f/D_B$,

Aspect ratio $AR=H/L$ .

Thermophysical properties of $Fe_3O_4$ nanoparticles and $H_2O$ are listed in Table 1.

**Table 1.** Thermophysical properties of $Fe_3O_4$ and $H_2O$ (Uddin *et al*. [29]).

| Thermophysical properties | $Fe_3O_4$ | $H_2O$ |
|---|---|---|
| $\rho$ [kgm$^{-3}$] | 5180 | 997.1 |
| $\mu$ [kgm$^{-1}$s$^{-1}$] | - | 0.001003 |
| $\kappa$ [Wm$^{-1}$K$^{-1}$] | 80 | 0.613 |
| $c_p$ [Jkg$^{-1}$K$^{-1}$] | 670 | 4179 |
| $\beta\times10^{-5}$ [K$^{-1}$] | 20.6 | 21 |
| Pr | - | 6.8377 |

The nanofluid motion is exhibited in terms of stream function $\psi$ that is obtained from the $x$- and $y$-components of the fluid velocity as follows:

$$U = \frac{\partial \psi}{\partial Y} \text{ and } V = -\frac{\partial \psi}{\partial X}. \tag{18}$$

To measure the heat transmission rate for engineering and technological applications it is essential to calculate the average Nusselt number. The Nusselt number at the bottom heated wall can be defined by

$$Nu = -Lk_f \left(\frac{\partial T}{\partial y}\right)_{y=0} / k_f \left(T_h - T_c\right). \tag{19}$$

The average Nusselt number in dimensionless form at the bottom heated wall is obtained as

$$Nu_{av} = -\int_0^1 \left(\frac{\partial \theta}{\partial Y}\right)_{Y=0} dX . \tag{21}$$

## 3. Numerical procedure

The dimensionless model equations (10)-(14) are highly nonlinear and coupled. It is difficult to solve them analytically for the closed form solutions. Thus, we solve them numerically for the approximate solutions. The finite element method of Galerkin type is a very powerful tool to handle these kinds of nonlinear equations. The details of this method can be found in the textbook by Zienkiewicz and Taylor [30] and in the work of Al Kalbani *et al*. [31]. The numerical simulation is carried out through the very robust pdf solver COMSOL Multiphysics. For grid independent results a widespread mesh testing is piloted for $Ra = 10^5$. Here, we examine five different non-uniform grids, named normal, fine, finer, extra fine, and extremely fine, consisting of 688, 1075, 1643, 7435 and 29157 elements in the resolution field respectively. To obtain convergent solutions, we calculate the average number at these grids to apprehend the grid refinement. Table 2 shows that $Nu_{av}$ for 7435 elements differs slightly from the value obtained for 14835 elements. To limit the computational time, it is sufficient to consider an extra fine grid consisting of 7435 elements for grid independent solutions.

**Table 2.** Grid sensitivity for $Fe_3O_4$-$H_2O$ nanofluid when $Ra = 10^5$.

| Nodes | 374 | 588 | 884 | 3850 | 14835 |
|---|---|---|---|---|---|
| Elements | 688 | 1075 | 1643 | 7435 | 29157 |
| $Nu_{av}$ | 7.0056 | 7.35383 | 7.65316 | 8.65204 | 8.66150 |

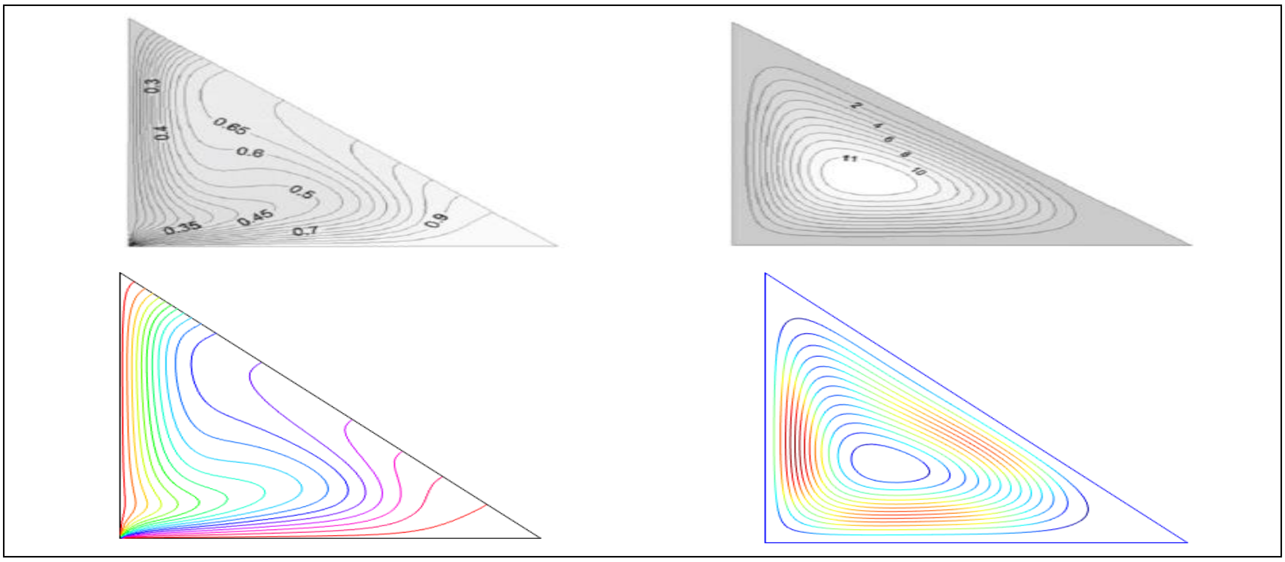


**Figure 2.** Judgment of isotherms (left column) and streamlines (right column) between Yesiloz and Aydin [11] (top row) and the present work (bottom row) when $Ra = 10^5$.

So as to check the correctness of our numerical scheme, we have validated it against the work of Yesiloz and Aydin [11] for a special case. Judgment of streamlines and isotherms between Yesiloz and Aydin [11] and the present work for $Ra = 10^5$ are depicted in Figure 2. The simulated results match each other profoundly which supports the use of the present numerical scheme.

## 4. Numerically simulated results and discussion

Here we present FEM generated numerical outcomes for convective flow of $Fe_3O_4$-$H_2O$ nanofluid confined in a right angle triangular enclosure under the accomplishment of a sloping magnetic field of varying updraft conditions at the bottom wall. Isotherms and average Nusselt number are calculated for a large assortment of the regulatory factors for three dissimilar cases as mentioned in section 2. Precise exertions were given to identify the role of the influential model parameters: $Ra$, $Ha$, $\gamma$ and $d$ on the flow and thermal fields. An enhanced heat transmission rate is predicted for homogeneously dispersed nanoparticles within the base fluid, but in reality the Brownian diffusion of nanoparticles and thermophoresis can create a tiny concentration difference ($\Delta C \approx 0.01$) within the flow domain. Following Uddin *et al.* [21] we obtain $D_B = 8.7591 \times 10^{-12}$, $D_T = 3.9597 \times 10^{-12}$, $Nb = 4.9591 \times 10^{-7}$, $Nt = 7.5229 \times 10^{-7}$ and $Le = 16795$ for $Fe_3O_4$-$H_2O$ nanofluid considering 1% nanoparticle loading when $d_p = 50\,\mathrm{nm}$, $T_c = 300\,\mathrm{K}$, and $\Delta T = 10\mathrm{K}$. The other model parameter values are taken as $\Pr = 6.8377$, $AR = 1$, $Nr = 0.01$ $Ha = 50$, $\gamma = \pi/12$, and $Ra = 10^6$ if not otherwise quantified.

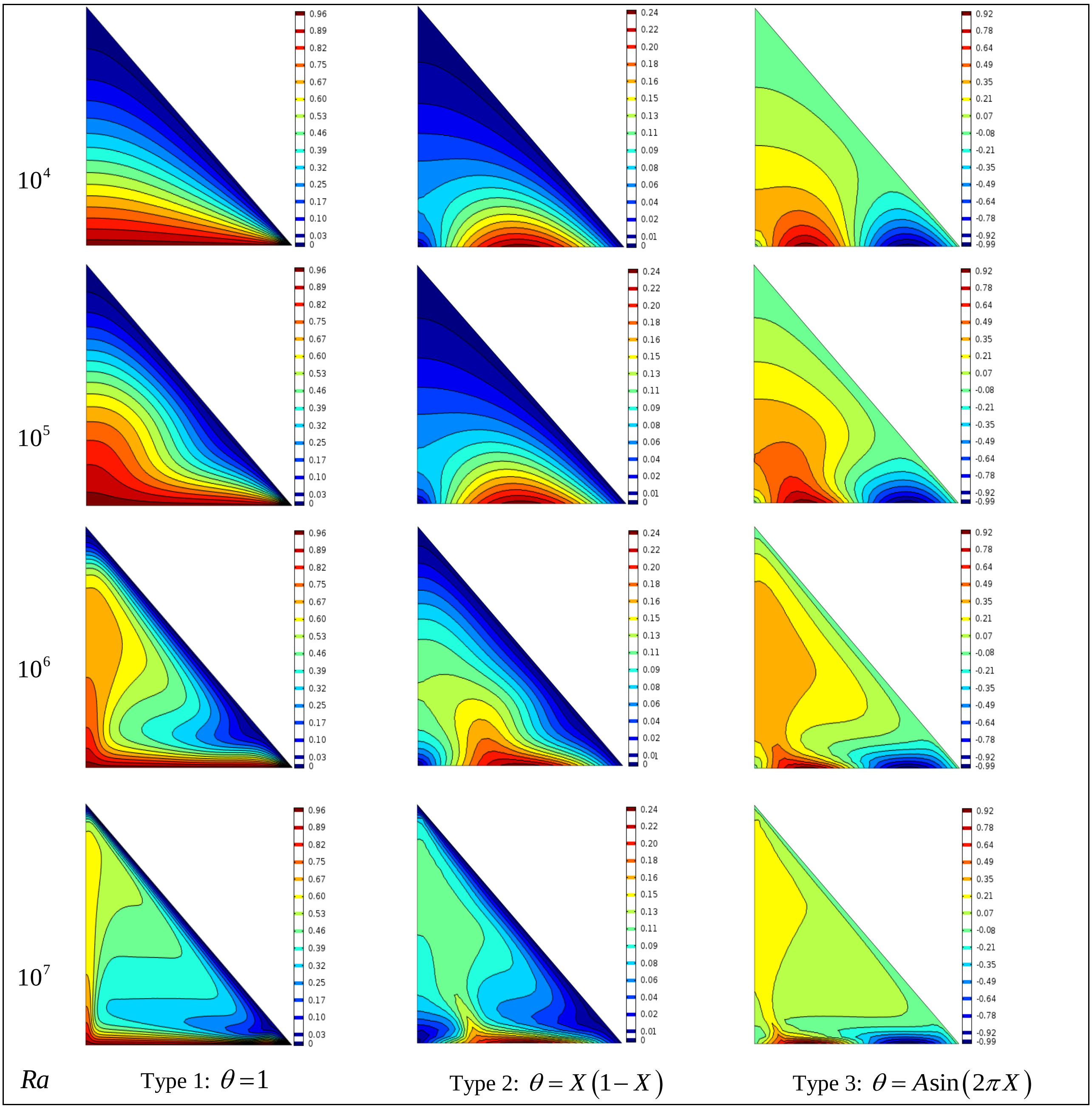


**Figure 3.** Distributions of isotherms for diverse $Ra$ and three different updraft conditions.

To measure the efficiency of heat transfer in $Fe_3O_4$-$H_2O$ nanofluid and determine the conductive to convective mode of heat transfer it is extremely useful to plot the isotherm contours. Figure 3 displays isotherm delineations for $Ra = 10^4$, $10^5$, $10^6$ and $10^7$ (top to bottom) for three different (Type 1, Type 2 and Type 3) updraft boundary conditions. These figures reveal that isotherm delineations are further compressed adjacent to the right junction of the lowermost wall of the cavity. The close concentration of isotherm contours in a region indicates that conduction is the key mode of heat transfer. As Rayleigh number increases, the compactness of the isotherm contours at the middle plane of the cavity decreases, which indicates a weaker mode of convective heat transport. A type 1 updraft boundary condition at the meeting point of hot and cold walls results in a finite discontinuity in the temperature distribution, as can be observed from Figure 3. Mathematically, it is a singularity, but in reality at this point the fluid temperature will converge towards the average value of the temperatures of hot and cold walls. Thus, in the simulation we have considered the average value of the temperatures at the right bottom corner point of the cavity for the Type 1 boundary condition (for a detailed discussion see Rahman *et al.* [27]). In contrast the implication of non-uniform updraft boundary conditions (Type 2 and Type 3) eliminates the thermal singularity, as evidenced from Figure 3. For all three types of thermal boundary conditions an increasing value of $Ra$ results in more distortion to the isotherms due to the resilient convection effect. Overall, an increase in $Ra$ enhances the heat transmission rate.

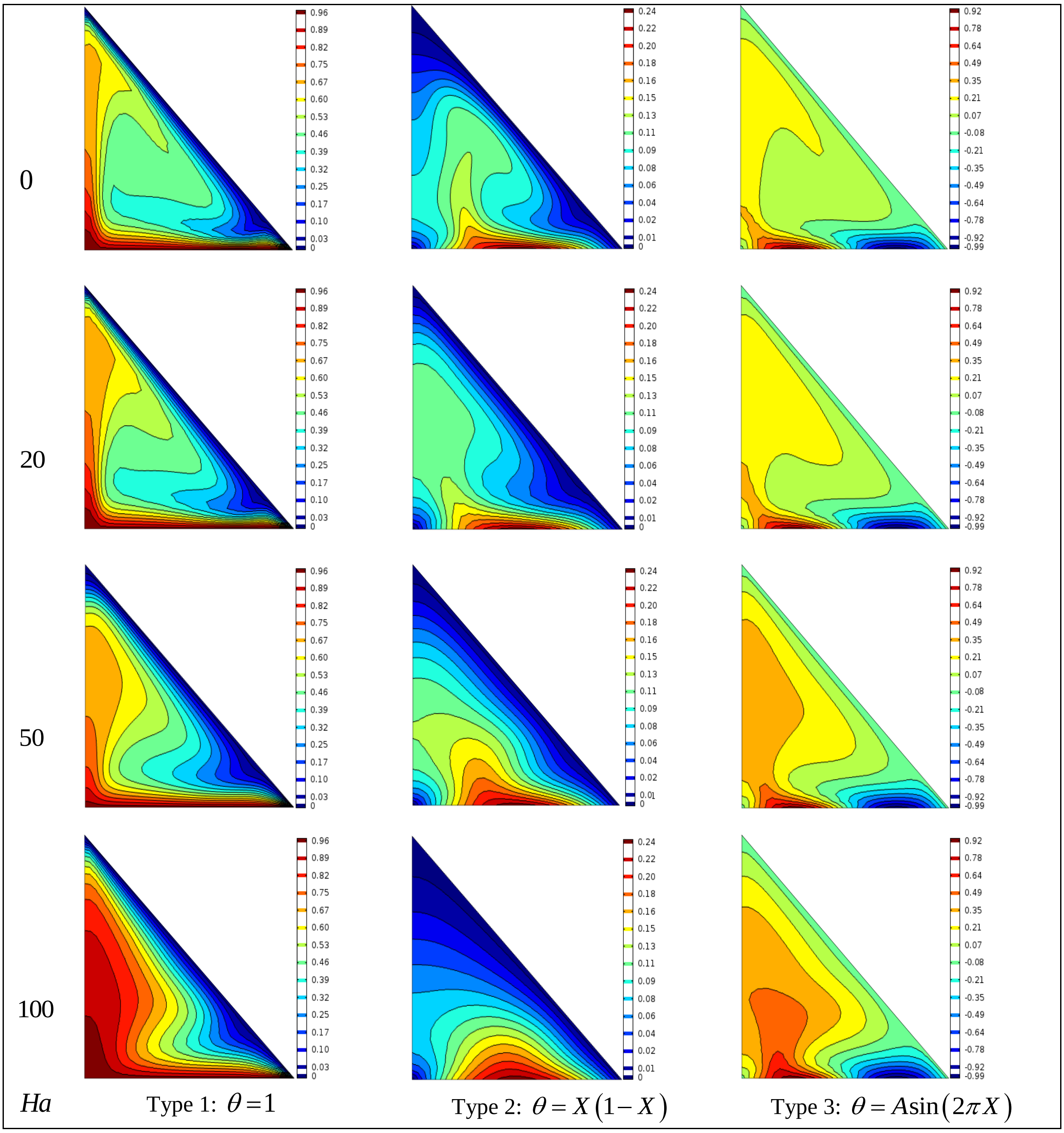


**Figure 4.** Distributions of isotherms for different $Ha$ and three different updraft conditions.

Meanwhile, Figure 4 depicts the impact of Hartmann number on the distributions of isotherms for various updraft boundary circumstances. These figures demonstrate that advanced temperature domain and clustered isotherms appear with a Type 1 thermal condition near the lowermost wall of the enclosure. This is due to the presence of a sharp temperature gradient along the vertical direction within the region. In contrast, in the upper region of the cavity, the temperature gradient is found to be quite weak for Type 2 and Type 3 thermal conditions. Nevertheless, in all cases of thermal boundary conditions an increased $Ha$, i.e. a stronger Lorentz force, pushes the densely distributed isotherm contours away from the hot wall. It signifies the decrease of the temperature rise within the enclosure. Thus, by using a magnetic field within the nanofluid flow domain we can control the heat transfer rate. In Figure 5 we display the influence of the magnetic field slopping angle $\gamma$ on the isotherm contours for $Fe_3O_4$-$H_2O$ nanofluid when $Ha$ is fixed. Figure 5 demonstrates that the influence of $\gamma$ on the temperature field is less pronounced. The isotherm contours are distributed quite evenly between the hot bottom and cold inclined walls of the cavity. The thickness of the thermal boundary layer is higher and the isotherms become more packed for a uniformly heated bottom wall compared to a non-uniformly heated one.

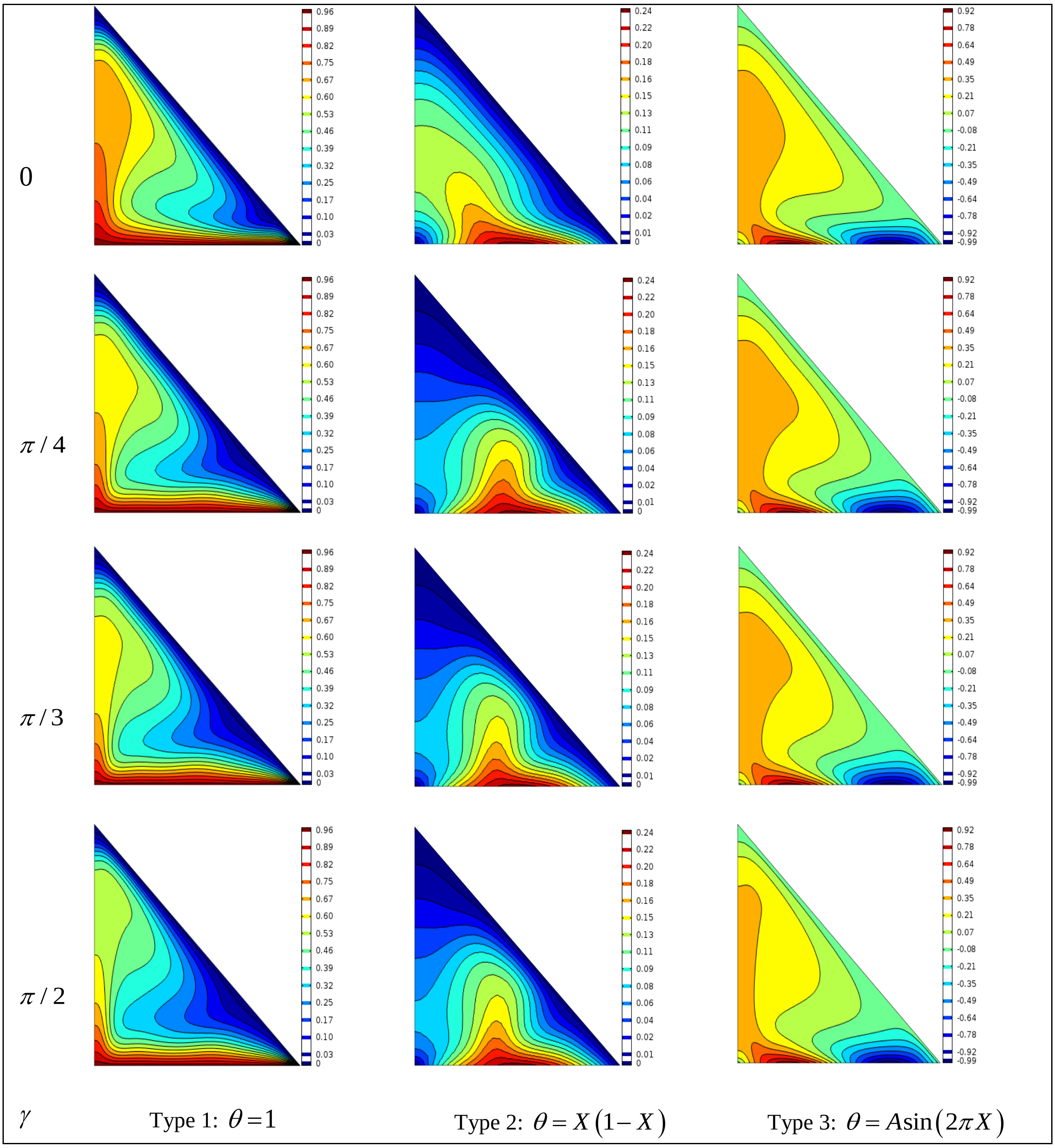


**Figure 5.** Distributions of isotherms for different $\gamma$ and three different updraft conditions.

To determine the heat transfer rate at the hot wall of the cavity filled with $Fe_3O_4$-$H_2O$ nanofluid for engineering applications we calculated the average Nusselt number varying $Ra$, $Ha$, $\gamma$ and $d_p$ in Table 3. This table reveals that average Nusselt number drops with the rise of $Ha$ i.e. a stronger magnetic force reduces the heat transfer rate. It also confirms that heat transmission in a nanofluid can be intensified by decreasing the nanoparticle size and increasing the buoyancy force. Table 3 further confirms that the highest heat transmission is achieved when the magnetic field sloping angle is $90^0$ and the bottom wall is heated uniformly.

**Table 3.** Values of $Nu_{av}$ for different model parameters and thermal boundary conditions (TBC).

| $d_p$ | $Ra$ | TBC | $Nu_{av}(Ha=0)$ | $Nu_{av}(Ha=100)$ | | |
|---|---|---|---|---|---|---|
| | | | | $\gamma=0^0$ | $\gamma=45^0$ | $\gamma=90^0$ |
| 1 | $10^5$ | Type 1 | 7.94847 | 6.71352 | 6.69363 | 7.27715 |
| | | Type 2 | 6.98167 | 5.81245 | 5.21564 | 6.45643 |
| | | Type 3 | 5.99345 | 3.93245 | 4.89654 | 5.34562 |
| | $10^6$ | Type 1 | 11.11553 | 8.96572 | 7.97159 | 9.69044 |
| | | Type 2 | 10.23421 | 7.43562 | 6.34521 | 8.43563 |
| | | Type 3 | 8.43567 | 5.23421 | 5.23456 | 6.34521 |
| | $10^7$ | Type 1 | 14.99211 | 15.10939 | 12.77243 | 14.93098 |
| | | Type 2 | 12.67543 | 14.23475 | 10.45638 | 12.43521 |
| | | Type 3 | 11.45632 | 10.45632 | 9.23451 | 11.21532 |
| 50 | $10^5$ | Type 1 | 6.98567 | 5.76543 | 5.45678 | 6.54321 |
| | | Type 2 | 5.99521 | 4.23421 | 4.12584 | 5.67543 |
| | | Type 3 | 4.99325 | 3.21456 | 3.02543 | 4.87654 |
| | $10^6$ | Type 1 | 10.45678 | 7.45632 | 6.78654 | 8.76549 |
| | | Type 2 | 9.45678 | 6.23457 | 5.67543 | 7.98654 |
| | | Type 3 | 7.34521 | 4.56743 | 4.12743 | 5.98765 |
| | $10^7$ | Type 1 | 14.97743 | 13.34563 | 11.34321 | 12.98765 |
| | | Type 2 | 11.97674 | 12.32156 | 9.76543 | 11.32854 |
| | | Type 3 | 10.96789 | 9.78654 | 8.98765 | 10.23784 |

## 5. Conclusion

The convective heat transfer mechanism in $Fe_3O_4$-$H_2O$ nanofluid confined in a right angled triangular cavity under the action of a slopping magnetic field has been investigated considering three types of thermal boundary conditions at the bottom wall of the cavity, following the mathematical model of Buongiorno. A very robust computer pde solver COMSOL Multiphysics which uses the FEM of Galerkin type was used to simulate the transformed non-dimensional equations governing the problem. An excellent agreement has been found among the data produced by the present code and those experimental data presented in the open literature. The simulated results were interpreted from a physical viewpoint. From the studied results we conclude that Rayleigh number is a key parameter that determines the mode of heat transfer. Lower $Ra$ determines conduction, whereas higher $Ra$ ($\geq Ra_{crit}$) corresponds to convection. An increased value of $Ra$ induces a heat transfer rate. The applied magnetic field eases $Nu_{ave}$ considerably through the Lorentz force. The magnetic field slopping angle regulates the flow configuration of $Fe_3O_4$-$H_2O$ nanofluid inside the cavity. A smaller particle size increases the heat transfer rate efficiently. The values of $Nu_{ave}$ are higher for a Type 1 condition compared to the Type 2 and Type 3 conditions. The highest rate of heat transfer is found when $\gamma=\pi/2$ and the bottom wall is heated uniformly.

## Acknowledgment

The author would like to thank the Sultan Qaboos University for funding through the research grant IG/SCI/DOMS/16/15.

## References

1. Kaushik, S.C., Kumar, R., Garg, H.P. and Prakash, J. Transient analysis of a triangular built-in-storage solar water-heater under winter conditions. *Heat Recovery Systems and Combined Heat and Power*, 1994, **14**, 337–341.

2. Asan, H. and Namli, L. Laminar natural convection in a pitched roof of triangular cross-section: summer day boundary conditions. *Energy and Buildings*, 2000, **33**, 69–73.
3. Omri, A., Orfi, J. and Nasrallah, J. B. Natural convection effects in solar stills. *Desalination*, 2005, **183**, 173–178.
4. Anandalakshmi, R. and Basak, T. Heat flow visualization in rhombic enclosures due to isothermal and non-isothermal heating at the bottom wall. *International Journal of Heat and Mass Transfer*, 2012, **55**, 325–1342.
5. Flack, R.D., Konopnicki, T. and Rooke, J.H. The measurement of natural convective heat transfer in triangular enclosures. *Journal of Heat Transfer*, 1979, **101**, 770–772.
6. Flack, R.D. The experimental measurement of natural convection heat transfer in triangular enclosures heated or cooled from below. *Journal of Heat Transfer*, 1980, **102**, 770–772.
7. Akinsete, V.A. and Coleman, T.A. Heat transfer by steady laminar free convection in triangular enclosures. *International Journal of Heat and Mass Transfer*, 1982, **25**, 991–998.
8. Ridouane, E.I., Campo, A. and Chang, J.Y. Natural convection patterns in right-angled triangular cavities with heated vertical sides and cooled hypotenuses. *Journal of Heat Transfer*, 2005,**127**, 1181–1186.
9. Varol, Y., Oztop, H.F. and Varol, A. Effects of thin fin on natural convection in porous triangular enclosures. *International Journal of Thermal Sciences*, 2008, **46**, 1033–1045.
10. Basak, T., Aravind, G. and Roy, S. Visualization of heat flow due to natural convection within triangular cavities using Bejan’s heatline concept. *International Journal of Heat and Mass Transfer*, 2009, **52**, 2824–2833.
11. Yesiloz, G. and Aydin, O. Laminar natural convection in right-angled triangular enclosures heated and cooled on adjacent walls. *International Journal of Heat and Mass Transfer*, 2013, **60**, 365–374.
12. Ozoe, H. and Okada, K. The effect of the direction of the external magnetic field on the three-dimensional natural convection in a cubical enclosure. *International Journal of Heat and Mass Transfer*, 1989, **32**, 1939-1954.
13. Pirmohammadi, M. and Ghassemi, M. Effect of magnetic field on convection heat transfer inside a tilted square enclosure. Int. Commun. *Heat Mass Transfer*, 2009, **36**, 776-780.
14. Sathiyammmoorthy, M. and Chamkha, A.J. Effect of magnetic field on natural convection flow in a liquid gallium filled square cavity for linearly heated side walls. *International Journal of Thermal Sciences*, 2010, **49**, 1856-1865.
15. Grosan, T., Renvic, C., Pop, I. and Ingham, D.B. Magnetic field and internal heat generation effects on free convection in a rectangular cavity filled with a porous medium. *International Journal of Heat and Mass Transfer*, 2009, **52**, 1525-1533.
16. Choi, S.U.S. Enhancing thermal conductivity of fluids with nanoparticles. In: Signier DA, Wang HP (eds.) Development and applications of non-Newtonian flows. *American Society of Mechanical Engineers Fluids Engineering Division*, vol.231/MD 1995, **66**, 99–105.
17. Wong, K.V. and De Leon, O. Applications of nanofluids: current and future. *Advances in Mechanical Engineering*, 2010; Article ID 519659 (11 pages).
18. Das, S.K., Choi, S.U.S., Yu, W. and Pradeep, T. Nanofluids: Science and Technology. *Wiley*, New Jersey, 2007.
19. Mahian, O., Kianifar, A., Kalogirou, S.A., Pop, I. and Wongwises, S. A review of the applications of nanofluids in solar energy. *International Journal of Heat and Mass Transfer*, 2013, **57**, 582–594.
20. Kakac, S. and Pramuanjaroenkij, A. Review of convective heat transfer enhancement with nanofluids. *International Journal of Heat and Mass Transfer*, 2009, **52**, 3187–3196.
21. Uddin, M.J., Al Kalbani, K.S., Rahman, M.M., Alam, M.S., Al-Salti, N. and Eltayeb, I.A. Fundamentals of nanofluids: evolution, applications and new theory. *International Journal of Biomathematics and Systems Biology*, 2015, **2** (1), 1-32.
22. Ghasemi, B. and Aminossadati, S.M. Mixed convection in a lid-driven triangular enclosure filled with nanofluids. *International Communications in Heat and mass Transfer*, 2010, **37**, 1142–1148.
23. Billah, M.M., Rahman, M.M., Razzak, M.A., Saidur, R. and Mekhilef, S. Unsteady buoyancy-driven heat transfer enhancement of nanofluids in an inclined triangular enclosure, *International Communications in Heat and Mass Transfer*, 2013, **49**, 115–127.
24. Al Kalbani, K.S., Rahman, M.M., Alam, M.S., Al-Salti, N. and Eltayeb, I.A. Buoyancy induced heat transfer flow inside a tilted square enclosure filled with nanofluids in the presence of oriented magnetic field. *Heat Transfer Engineering*, *2018*, **39**, 511-525.
25. Buongiorno, J. Convective transport in nanofluids. *Journal of Heat Transfer*, 2006, **128**, 240-250.
26. Sheremet, M.A. and Pop, I. Free convection in a triangular cavity filled with a porous medium saturated by a nanofluid; Buongiorno's mathematical model. *International Journal of Numerical Methods for Heat and Fluid Flow*, 2015, **25**, 1138-1161.
27. Rahman, M.M., Alam, M.S., Al-Salti, N. and Eltayeb, I.A. Hydromagnetic natural convective heat transfer flow in an isosceles triangular cavity filled with nanofluid using two-component nonhomogeneous model. *International Journal of Thermal Sciences*, 2016, **107**, 272-288.
28. Elshehabey, H.M. and Ahmed, S.E. MHD mixed convection in a lid-driven cavity filled by a nanofluid with sinusoidal temperature distribution on the both vertical walls using Buongiorno's nanofluid model. *International Journal of Heat and Mass Transfer*, 2015, **88**, 181–202.

29. Uddin, M.J., Rahman, M.M. and Alam, M.S. Analysis of natural convective heat transport in homocentric annuli containing nanofluids with an oriented magnetic field using nonhomogeneous dynamic model, *Neural Computing and Applications*, 2017. DOI 10.1007/s00521-017-2905-z.
30. Zienkiewicz, O.C. and Taylor, R.L. The finite element method (4$^{th}$ Edition), *McGraw-Hill*, 1991.
31. Al Kalbani, K.S. Alam, M.S. and Rahman, M.M. Finite element analysis of natural convective heat transfer flow of nanofluids inside a tilted square enclosure in the presence of oriented magnetic field. *American Journal of Heat and Mass Transfer*, 2016, **3(3)**, 186-224.

Received 28 December 2017
Accepted 2 February 2018